UCRL-JC-125402
PREPRINT

Structure of Mix in a Rayleigh-Taylor Unstable Fluid Cell

M. B. Schneider
G. Dimonte
B. A. Remington

This paper was prepared for submittal to the
6th International Workshop on the Physics of Compressible Turbulent Mixing
Marseille, France
June 18-21, 1997

September 2, 1997

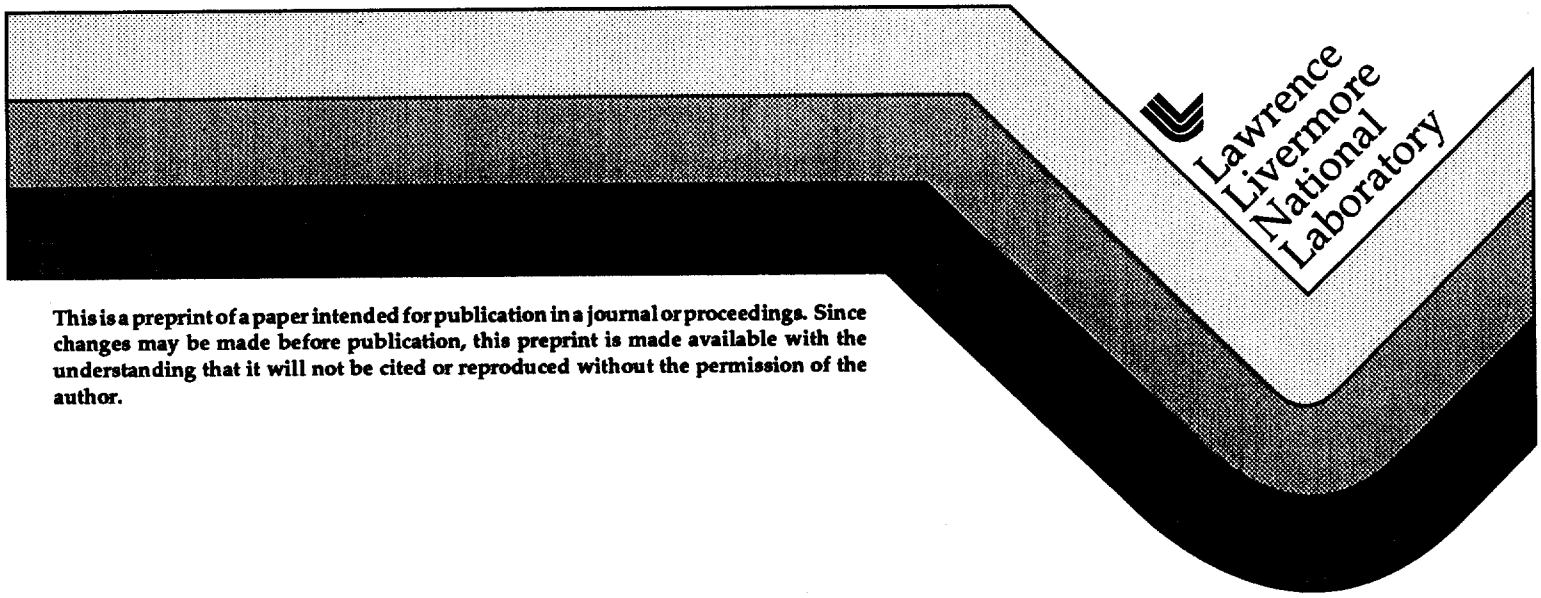

Structure of Mix in a Rayleigh-Taylor Unstable Fluid Cell

Marilyn B. Schneider, Guy Dimonte, and Bruce A. Remington
Lawrence Livermore National Laboratory
P. O. Box 808, L-43, Livermore, CA 94550 USA

Abstract: Laser-induced fluorescence is used to image the central plane of the mix region of two immiscible liquids subject to the Rayleigh-Taylor instability. The familiar bubbles and spikes display a complex internal structure. This small-scale structure creates a large contact area whose density is constant in time. The size of the mixing zone, defined in a new way, grows with coefficient $\alpha_b >= 0.054$.

1. Introduction

The Rayleigh-Taylor (RT) instability[1, 2, 3, 4], occurs during the acceleration of a heavy fluid by a light fluid. The rate of the instability is parameterized by the acceleration, g, and the Atwood number, $A=(\rho_2 - \rho_1)/(\rho_2 + \rho_1)$ where $\rho_1(\rho_2)$ is the density of the light (heavy) fluid. For small initial perturbations, there are linear[2, 6] and non-linear growth phases[5, 7, 8, 9]. Eventually a highly-disordered mixing zone (DMZ) develops, bounded by a bubble front which penetrates the heavy fluid as $\sim \alpha_b Agt^2$ and a spike front which penetrates the light fluid as $\sim \alpha_s Agt^2$. [10, 11, 12, 13, 14, 15] The coefficient α_b is insensitive to A whereas α_s increases with A[13, 14].

Experiments[10, 11, 12, 15] using backlit photography obtain values of $\alpha_b \sim 0.06 - 0.07$ that are larger than those found in all 3-D [13, 16] and some 2-D [12, 16, 17] hydrodynamic simulations, but similar to those found in 2-D simulations which track the interface [18, 19]. The backlit photography experiments cannot measure the structure within the DMZ. This structure is important because it determines the constitutive properties in the DMZ such as composition (or density), energy, effective opacity, and equation of state.

This report describes RT experiments using laser-induced fluorescence (LIF) which image the DMZ of a cell containing two immiscible liquids at Reynolds number of order $\sim 10^5$. The images show a complex internal fine structure in the bubbles and spikes. While the large bubbles and spikes define the boundaries of the DMZ, their small-scale internal structures increase the mix entropy, which eventually (for miscible fluids) leads to molecular mix. This study shows that: (i) the measured α_b is consistent with recent experiments[15]; and (ii) the internal structure is responsible for the large amount of contact area between the mixing fluids.

2. Experimental configuration

The present experiments use the Linear Electric Motor (LEM) [20] at Lawrence Livermore National Laboratory to accelerate a container for 50 ms at a downward constant g ($\sim 73 g_0$ where g_0 = earth's gravity). The fluid cavity is 73mm wide, 88 mm high, and 73mm deep. For LIF, a laser sheet parallel to the acceleration illuminates the central plane of the cavity from below. Images of the fluorescence are recorded on 35mm film.

[0]More information - Email: schneider5@llnl.gov

The film images are digitized, converted to intensity images, corrected for the absorption of the laser light by dye molecules in the fluid, smoothed to reduce noise, and adjusted for variations in the laser beam intensity across the cell. To avoid wall effects, only the central 62 mm width of the cell is analyzed.

The fluids are decane ($\rho_1 = 0.73$ g/cm^3), and salt water ($\rho_2 = 1.43$ g/cm^3) plus a small amount of fluorescent dye (Kiton Red 620), giving an Atwood number of $A = 0.34$. The surfactant AOT is added to lower the interfacial tension to ultra-low values by forming a microscopically-thin microemulsion phase [21] at the interface. Glucose is added to the salt water to match its refractive index to within 0.03% of that of decane.

3. Experimental results

Corrected film density images at 27 and 45 ms are shown in the first column of Figure 1. The

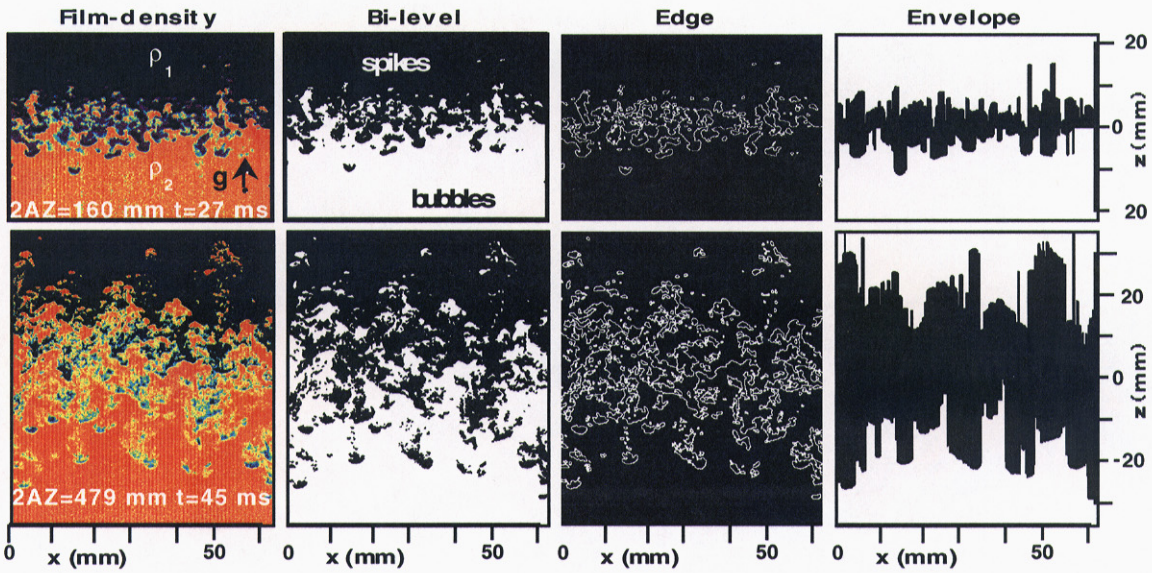

Figure 1. Images from a single run at two times illustrating the various types of processed images. The corrected film-density images are used to generate the bi-level images . The bi-level images are used to generate the edge images and the envelope images.

net displacement of the cell due to the acceleration is Z and the generalized displacement is defined as $Agt^2 = 2AZ$. The planar coordinate system moving with the fluid cell is x, z, with z=0 at the original interface.

The interfacial tension, σ, stabilizes the RT growth of perturbations with small wavelengths, leading to a mode of fastest growth with wavelength $2\pi\sqrt{(3/2)}L_c$ where L_c is the capillary length, $L_c^2 = 2\sigma/[(\rho_2 - \rho_1)g]$. [22] In the present experiment, L_c=0.10 mm at 73 g_0 so the fastest growing wavelength is ~0.7 mm with an e-folding time[22] ~0.9ms. When the amplitude becomes $\sim 1/k \sim 0.1$mm, the mode saturates. Thus, by 27 ms (the top image in Figure 1), the system has evolved into the DMZ regime.

The images are processed into bi-level and edge images to emphasize the internal structures, and envelope images, which display the large-scale features. This is shown in Figure 1. The bi-level image is generated from the corrected film-density image by mapping all pixels with less than ~50% intenstiy to 0, and all pixels with greater than ~50% intensity to 100. The actual cutoff level used for the mapping is adjusted to keep about the same number of pixels in each

fluid (conservation of volume). The bi-level image is used to generate (i) the edge image using the Roberts Edge method[23] and (ii) the envelope image using single-valued (in x) bubble and spike envelopes. The lower (bubble) envelope function is obtained by finding the value of z at which the maximum penetration of the top fluid into the bottom fluid occurs. The spike envelope is similar but on top. In the envelope image, the region between the two envelope functions is shown in black to mimick the backlit photographs[10, 11, 12, 15]. The resolution of the processed images is $< 1mm$ [24].

3.1. The growth of the mix region (DMZ)

The width of the DMZ is obtained from the bi-level image. Backlit photographs[10, 11, 12, 15] obtain the width by measuring the penetration of the bubble- and spike-fronts. The present data samples only one plane of the DMZ, so fewer bubbles and spikes are observed. To overcome the reduced statistics, a new penetration depth is defined from the projection of the bi-level image onto the z axis, as shown in Figure 2. The projection is plotted as a density profile and

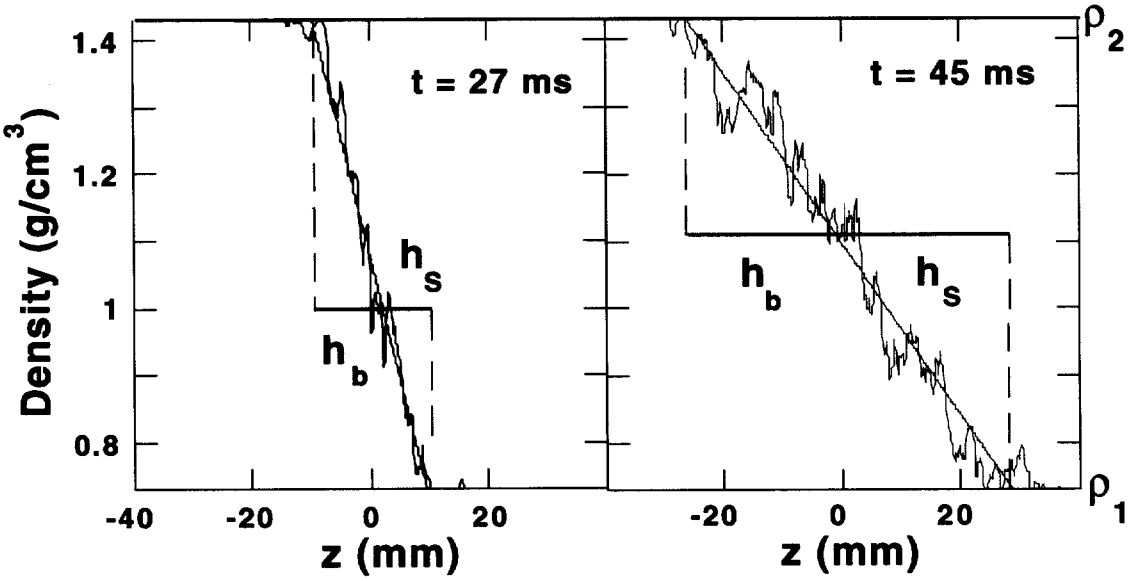

Figure 2. The projection of the bi-level images of Figure 1 onto the z axis. The projection is normalized to the density of the fluids. The definitions of bubble (h_b) and spike (h_s) penetration distances are shown.

generally has many fluctuations, so it is fit to a straight line. The bubble (spike) penetration, h_b, (h_s) is defined as the distance between the intersection of the straight line with $\rho_2(\rho_1)$ and the original location of the flat interface (z=0). The latter can be measured to within ~1mm. The present definitions of h_b and h_s are statistically robust because they depend on the entire profile. A procedure could have been employed which defines $h_b[h_s]$ by the $\rho_1 + 0.95(\rho_2 - \rho_1)[\rho_1 + 0.05(\rho_2 - \rho_1)]$ point of the profile, but the results would be too sensitive to fluctuations in the projections.

The variation of h_b and h_s with generalized displacement 2AZ appears linear, as shown in Figure 3, implying a self-similar evolution. This collection of data represents 6 separate runs, recording three images per run. The errors are the same size as the plot symbols and are due to the uncertainty in the location of the original interface. The data are fit to straight lines[10, 17], $h = h_0 + \alpha$ 2AZ. The linear fits in Figure 3 give $\alpha_b = 0.054 \pm 0.003$ and $\alpha_s = 0.062 \pm 0.003$. The value of α_b is ~10% smaller than the value obtained in backlit photography. This is expected

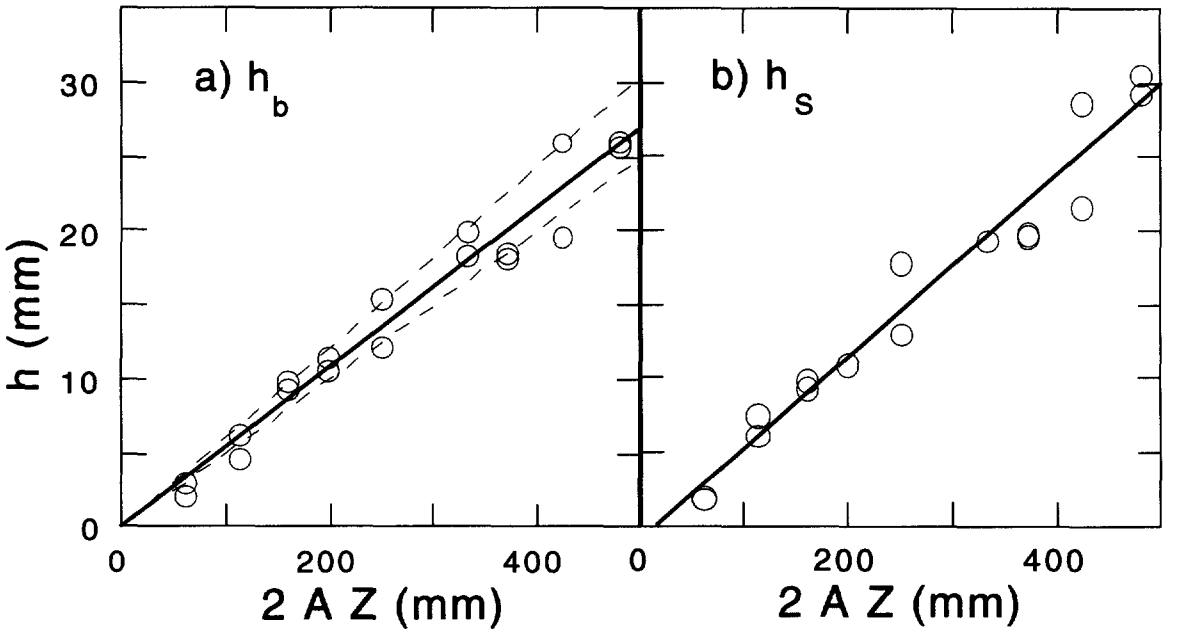

Figure 3. (a) Bubble, h_b, and (b) spike, h_s, penetrations vs. generalized displacement, 2AZ. The solid lines are (a) h_b= -0.45 + 0.054 2AZ and (b) h_s= -0.95 + 0.062 2AZ. The dashed lines in (a) show α_b= 0.061 (upper line) and 0.05 (lower line).

because the laser sheet may not illuminate the most penetrating bubbles or spikes or their tips. This effect is greater later in time when there are only a small number of bubbles (2-4) with large penetrations. The upper dashed line in Figure 3a shows the backlit photography result[15], h_b= 0.061 2AZ. This line is consistent with the early-time data ($2AZ < 200$) and with the most-penetrating late-time data. Thus, the results indicate that backlit photography is not seriously contaminated by wall effects. The measured α_b is ~5% higher than those found in 3-D hydrodynamic simulations [13, 16]. The lower dashed line in Figure 3a shows the simulation result, h_b = 0.05 2AZ. The simulations obtain h_b and h_s from the 99%, 1% [13] points of a volume-fraction profile. The simulation results may be slightly low. One difference is that the experiments use immiscible fluids whereas the fluids in the simulations are miscible.

Finally, the ratio h_s/h_b, obtained from the data in Figure 3, is $h_s/h_b = 1.1 \pm 0.05$. The error bars reflect the sensitivity of this ratio to the location of the flat interface. This ratio is in agreement with previous data (see figure 8 in Ref. [19]) and one 3-D simulation[13] but lower than the 1.3 predicted from another 3-D simulation[19] and lower than the 1.3 [19] to 1.4 [14]that models predict for A=0.34.

3.2. Structure of the DMZ

The contact area between the mixing fluids, shown in the edge images of Figure 1, determines the degree of particle and energy exchanges. In the 2-D edge image, the contact area is the length of the white pixels. The two edge images in Figure 1 display similar densities of white pixels in the centers of their respective DMZs, implying some small scale structure is always present. The edge images will be analyzed in another publication [24]. Models[9, 14, 18, 25, 26, 27] predict the evolution of the boundaries of the DMZ to larger structure sizes. Larger structures have a smaller perimeter density than smaller structures, so processes not included in the models appear to be occuring which maintain the density of the small-scale structures.

The images in Figure 1 do suggest, however, that a large lengthscale increases with time. This lengthscale, associated with the width and separation of the bubble and spike fronts, is seen most clearly in the envelope images. Notice the bubbles and spikes are long and skinny in these images. It will be discussed in a future publication [24].

4. Summary

In summary, images of the central plane of an RT unstable fluid cell are analyzed and give mix widths that agree with those obtained using the backlit photography technique[15], implying that the latter are not hampered by window effects. The present study uses a statistically robust definition for h_b and h_s and finds lower limits on $\alpha_b = 0.054 \pm 0.003$ and $\alpha_s = 0.062 \pm 0.003$, consistent with recent backlit photography experiments[15] (α_b= 0.061). The present results are still somewhat higher than in 3-D simulations (α_b(3D) = 0.04-0.05) [13, 16]. In addition, late in time, the bubbles and spikes are seen to maintain a complicated internal fine structure, as predicted in some numerical simulations[12, 19, 29] and models[28]. In contrast, the width of the large-scale features (bubbles and spikes) appear to grow in time[28].

Acknowledgement. We thank J. Ticehurst, S. Kiar, D. Nelson, S. Weaver, C. Allison, and T. Schwinn for their expert technical contributions. We are grateful to Drs. E. Burke, T. Clark, F. Harlow, P. L. Miller, D. Saltz, D. H. Sharp, A. Shestakov, D. Shvarts, P. Stry, D. Youngs, and Q. Zhang for invaluable discussions. We thank Dr. M. Eckart for his support. This work was performed under the auspices of the U.S. Department of Energy by the Lawrence Livermore National Laboratory under Contract No. W-7405-ENG-48.

References

[1] Lord Rayleigh, *Scientific Papers, Vol. II* (Cambridge Univ. Press, Cambridge, England, 1900).
[2] G. Taylor, Proc. Roy. Soc. A **201**, 192 (1950).
[3] E. Muller, B. Fryxell, and D. Arnett, Astron. Astrophys. **251**, 505 (1991); M. Herant and S. E. Woosley, Astrophys. J. **425**, 814 (1994).
[4] J.D. Lindl and W.C. Mead, Phys. Rev. Lett. **34**, 1273 (1975); J.D. Kilkenny *et al.*, Phys. Plasmas **1**, 1379 (1994).
[5] B. A. Remington et al., Phys. Plasmas **2**, 241 (1995).
[6] D.J. Lewis, Proc. Roy. Soc. A **202**, 81 (1950); J. W. Jacobs and I. Catton, J. Fluid Mech. **187**, 353 (1988).
[7] M.J. Dunning and S. Haan, Phys. Plasmas **2**, 166 (1995).
[8] D. Ofer *et al.*, Phys. Fluids B **4**, 3549 (1992).
[9] D.H. Sharp, Physica D **9**, 3 (1984).
[10] K.I. Read, Physica D **12**, 45 (1984).
[11] Y.A. Kucherenko et al., in *3rd Int'l Workshop on The Physics of Compressible Turbulent Mixing* Abbey of Royaumont, Fr. June 1991. p 427
[12] D.L. Youngs, Physica D **37**, 270 (1989).
[13] D. L. Youngs, Phys. Fluids A **3**, 1312 (1991).
[14] U. Alon *et al.*, Phys. Rev. Lett. **74**, 534 (1995).
[15] G. Dimonte and M. Schneider, Phys. Rev. E **54**, 3740 (1996).
[16] J. Hecht et al., Laser and Particle Beams **13**, 423 (1995).
[17] S. Atzeni and A. Guerrieri, Europhysics Lett. **22**, 603 (1993).
[18] J. Glimm *et al.*, Phys. Fluids A **2**, 2046 (1990).
[19] N. Freed *et al.*, Phys Fluids A **3**, 912 (1991).

[20] G. Dimonte *et al.*, Rev. Sci. Inst. **67**, 302 (1996).
[21] R. Aveyard *et al.*, J. Chem Soc., Faraday Trans. 1 **82**, 125 (1986).
[22] R. Bellman and R. H. Pennington, Q. Appl. Maths **12**, 151 (1954).
[23] John C. Russ, *The Image Processing Handbook* (CRC Press, Inc.,1995) 233-249; chapter 5.
[24] M.B. Schneider, G. Dimonte, B. Remington (in preparation)
[25] J. A. Zufiria, Phys. Fluids **31**, 440 (1988); U. Alon *et al.*, Phys. Rev. Lett. **72** 2867 (1994); X.L. Li, Phys. Fluids **8**, 336 (1996).
[26] J. Glimm and D. H. Sharp, Phys. Rev. Lett. **64**, 2137 (1990); Q. Zhang, Phys. Lett. A **151**, (1990).
[27] David Saltz, private communication (1997)
[28] K. O. Mikaelian, Physica D **36**, 343 (1989).
[29] See images at http://esd.gsfc.nasa.gov/ESS/annual.reports/ess95contents/app.inhouse.fryxell.html

Technical Information Department • **Lawrence Livermore National Laboratory**
University of California • Livermore, California 94551